Water Research 130 (2018) 200–207

Contents lists available at ScienceDirect

Water Research

journal homepage: www.elsevier.com/locate/watres

Oxidation of iopamidol with ferrate (Fe(VI)): Kinetics and formation of toxic iodinated disinfection by-products

Huiyu Dong [a], Zhimin Qiang [a, *], Shaogang Liu [b], Jin Li [c], Jianwei Yu [a], Jiuhui Qu [a]

[a] Key Laboratory of Drinking Water Science and Technology, Research Center for Eco-Environmental Sciences, University of Chinese Academy of Sciences, Chinese Academy of Sciences, 18 Shuang-qing Road, Beijing, 100085, China
[b] Guangxi Colleges and Universities Key Laboratory of Food Safety and Pharmaceutical Analytical Chemistry, Guangxi Key Laboratory of Chemistry and Engineering of Forest Products, School of Chemistry and Chemical Engineering, Guangxi University for Nationalities, 158 Da-xue Road, Nanning, 530006, Guangxi, China
[c] School of Environmental Science and Engineering, Qingdao University, 308 Ning-xia Road, Qingdao, 266071, China

ARTICLE INFO

Article history:
Received 3 September 2017
Received in revised form
13 November 2017
Accepted 4 December 2017
Available online 5 December 2017

Keywords:
Ferrate
Iopamidol
Kinetics
Iodinated disinfection by-products

ABSTRACT

Presence of iodinated X-ray contrast media (ICMs) in source water is of high concern, because of their potential to form highly toxic iodinated disinfection by-products (I-DBPs). This study investigated kinetics, mechanisms and products for oxidation of one ICMs, iopamidol (IPM) by ferrate (Fe(VI)). The obtained apparent second-order rate constants for oxidation of IPM by Fe(VI) ranged from 0.7 M^{-1} s^{-1} to 74.6 M^{-1} s^{-1} at pH 6.0–10.0, which were highly dependent on pH. It was found that the oxidation of IPM by Fe(VI) led to the formation of highly toxic I-DBPs. Iodoform (IF), iodoacetic acid and triiodoacetic acid formations were observed during the oxidation and IF dominated the formed I-DBPs. The formation of I-DBPs was also governed by pH and the maximum formation of I-DBPs occurred at pH 9.0. Transformation pathways of IPM by Fe(VI) oxidation were speculated to proceed through deiodination, amide hydrolysis and oxidation of amine reactions. The deiodination reaction during the oxidation of IPM by Fe(VI) contributed to the formation of I-DBPs. The formation of I-DBPs during the oxidation of IPM by Fe(VI) was significantly higher than those of iohexol, diatrizoate and iopromide, which was consistent with the lowest molecular orbital energy gap of IPM. Although Fe(VI) is considered as a green oxidant, the formation of highly toxic I-DBPs during the oxidation of IPM should receive great attention.

1. Introduction

Iodinated X-ray contrast media (ICMs) are widely administrated to image soft tissues during diagnostic tests. These pharmaceuticals are metabolically stable in the body and can be discarded rapidly via urine and feces. It has been reported that up to 120 g of ICMs are used per application with approximately 75 million patient applications annually (Christiansen, 2005). As conventional wastewater treatment plants (WWTPs) cannot remove ICMs effectively, they have been detected widely in WWTPs effluents, surface water and even drinking water (Seitz et al., 2006; Perez and Barcelo, 2007). Four kinds of ICMs have been detected in an occurrence study of source waters from 10 cities in the United States and iopamidol (IPM) was the most frequently detected media with concentrations up to 2.7 μg L^{-1} (Duirk et al., 2011). Additionally, 98 ng L^{-1} of IPM was found in the finished drinking water in European waterworks (Seitz et al., 2006), which is a few orders of magnitude higher than those of many other micro-pollutants (Simazaki et al., 2015).

Because of the biological recalcitrance of IPM, continued physicochemical efforts including ozone, γ-irradiation, radical oxidation and ultrasound have been made to degrade IPM from water (Ning and Graham, 2008; Seitz et al., 2008; Jeong et al., 2010; Wendel et al., 2014; Simazaki et al., 2015; Dong et al., 2017a). The removal of IPM, however, inevitably is accompanied by the formation of products or disinfection by-products (DBPs) that potentially can be even more toxic than the parent compound (Matsushita et al., 2015; Wendel et al., 2016). For example, it was reported that a deiodination reaction usually occurred during the oxidation of ICMs, which primarily resulted in the oxidation of the side chains (Seitz et al., 2008; Eversloh et al., 2014). The deiodination reaction may induce the release of inorganic iodine from ICMs, which becomes a potential iodine source of iodinated DBPs (I-DBPs) during

* Corresponding author.
E-mail address: qiangz@rcees.ac.cn (Z. Qiang).

https://doi.org/10.1016/j.watres.2017.12.003
0043-1354/

oxidation or disinfection (Wendel et al., 2016).

The iodine present in the source water could be oxidized to hypoiodous acid (HOI) by oxidant, which rapidly incorporates into any organic matter present and induces the formation of I-DBPs (Liu et al., 2017). During the past decade, it was verified that I-DBPs generally are more cytotoxic, genotoxic and developmental toxic than their brominated or chlorinated analogs (Richardson et al., 2008; Yang and Zhang, 2013). As the mass fraction of iodine in IPM molecular is up to 50%, IPM not only contributes substantially to total organic iodine in water, but also acts as a potential iodine source for the formation I-DBPs. Previous studies have identified 46 biotransformation products of iopromide, iohexol, iomeprol, and IPM from aerobic soil, water and sediment-water systems (Schulz et al., 2008; Kormos et al., 2009, 2010). These products, which still contain iodine in their structures, may become potential sources of the iodine in formation of I-DBPs during disinfection (Duirk et al., 2011). Thus, the products of IPM during oxidation should receive great attention for toxicity evaluation.

With oxidizing power higher than those of the common oxidants (e.g., permanganate, ozone, and hypochlorite), ferrate (Fe(VI)) could react with electron-rich organic moieties including phenols, anilines, amines, estrogens and pharmaceuticals (Sharma et al., 2001; Anquandah et al., 2011; Dong et al., 2017b). Meanwhile, Fe(VI) has excellent disinfectant properties and can inactivate a wide variety of microorganisms at low Fe(VI) dosages. It was reported that Fe(VI) could inactivate *Escherichia coli* at lower dosages or shorter contact time than hypochlorite. Fe(VI) can also kill many chlorine resistant organisms including aerobic spore-formers and sulphite-reducing clostridia (Sharma, 2007). Moreover, the reaction of Fe(VI) promotes the coagulation process, and subsequently forms a ferric hydroxide gel, which could greatly enhance the aggregation and settling process (Jiang and Wang, 2003). Thus Fe(VI) is considered as a green oxidant for water and wastewater treatment.

It has been accepted that Fe(VI) is one of the few oxidants that seldom forms halogenated hazardous byproducts. Interestingly, Kralchevska et al. (2016) found that Fe(VI) could oxidize iodide (I^-) into I_3^- in the presence of excess I^-. More importantly, formed I_3^- may react with natural organic matter to yield I-DBPs. Thus, it would be meaningful to investigate whether or not toxic I-DBPs form during the oxidation of IPM by Fe(VI), which could provide new insight for toxicity evaluation after Fe(VI) oxidation. In this study, the oxidation kinetics of IPM by Fe(VI) was firstly investigated at different pHs. Then, the formation of I-DBPs including iodoform (IF), iodoacetic acid (IAA) and triiodoacetic acid (TIAA) during the oxidation of IPM by Fe(VI) was evaluated under different water qualities. The high-molecular-weight transformation byproducts (TBPs) of IPM by Fe(VI) were also identified, and on this basis, the potential degradation pathways were proposed. Besides, the formation of I-DBPs during the oxidation of other three ICMs by Fe(VI) was further investigated. For the first time, this study verified the formation of toxic I-DBPs during the oxidation of IPM by Fe(VI), which helps to better understand the product and toxicity evolution of emerging ICMs during Fe(VI) oxidation.

2. Materials and methods

2.1. Materials

IF (99%), IAA (98%), TIAA (90%), K_2FeO_4 (97%), iopamidol (99%), iohexol (99%), sodium diatrizoate hydrate (99%) and iopromide (99%) were obtained from Sigma Aldrich (St. Louis, MO, USA). An internal standard of 1,2-dibromopropane were purchased from J&K Chemical Co. (Beijing, China). Acetonitrile and methanol were purchased from Thermo Fisher Scientific (Waltham, MA, USA)) at high-performance liquid chromatography (HPLC) grade purity and formic acid (≥99.0%) was from Dikma Technologies (Lake Forest, CA, USA). Suwannee River NOM isolate (2R101N) was obtained from the International Humic Substances Society. Ammonium sulfate (99%) and NaOCl (5% of active chlorine) were obtained from Sinopharm Chemical Reagent Co. (Shanghai, China). All other chemicals of at least analytical grade were provided by Beijing Chemical Reagents Company (Beijing, China). Purified water (18 MΩ cm) was obtained from a Milli-Q system (Advantage A10, Millipore, Billerica, MA, USA).

2.2. Experimental procedures

2.2.1. Kinetics

Kinetic experiments were conducted in 250 mL brown glass reactors in batch mode at ambient temperature (25 °C). A certain volume of Fe(VI) stock solution was added to the reactor containing IPM with a total volume of 100 mL. Typically, the initial experimental doses of IPM and Fe(VI) were 10 μM and 0.1 mM Fe(VI), respectively. A relatively high initial concentration of IPM was adopted for kinetic determination and TBP identification. The stock solutions of Fe(VI) (1–5 mM) were freshly prepared by dissolving solid K_2FeO_4 in pH 9.1 buffer (5 mM Na_2HPO_4/1 mM borate), which was determined by measuring Fe(VI) absorbance at 510 nm ($\varepsilon_{510nm} = 1150\ M^{-1}\ cm^{-1}$) (Rush et al., 1996). 10 mM Na_2HPO_4 buffer was used for pH 6.0–8.0 and 5 mM Na_2HPO_4/1 mM borate buffer was used for pH 9.0–10.0. The kinetic experiments usually lasted 30 min and aliquots (1.0 mL each) of reaction solution were withdrawn at predetermined time intervals, quenched with $Na_2S_2O_3$ ($[S_2O_3^{2-}]$:$[Fe(VI)]_o$ molar ratio = 2.0), filtered through 0.2 μm polyethersulfone filters (ion chromatography acrodisc, PALL) and analyzed for residual IPM concentration. Each experiment was conducted in triplicate, and the mean values were reported with error bars representing the 95% confidence interval.

2.2.2. Formation of I-DBPs

The formation of I-DBPs during the oxidation of IPM by Fe(VI) of was studied as a function of reaction time, pH, IPM concentration and NOM concentration. All experiments were performed in triplicate using 50-mL amber glass bottles with polytetrafluoroethylene-lined septum screw-caps under headspace-free conditions. The pH of all reaction solutions was controlled at 9.0 ± 0.1 with 5 mM Na_2HPO_4/1 mM borate buffer except when the effect of pH was examined. Similar experimental procedures were adopted when testing the formation of I-DBPs during the oxidation of other three ICMs by Fe(VI). Generally, I-DBP formation experiments lasted 72 h to examine the I-DBP formation potential. After 72 h, 20 mL water samples were withdrawn and quenched with $Na_2S_2O_3$, ($[S_2O_3^{2-}]$:[Fe(VI)] molar ratio = 2.0) to quench the residual Fe(VI). Water samples were extracted and analyzed immediately after quenching to prevent potential hydrolytic loss of byproducts during storage.

2.2.3. Formation of I-DBPs in real waters

To investigate I-DBP formation during the oxidation of IPM by Fe(VI) in real waters, 500 μg L^{-1} IPM was spiked into three real waters including the river water from Miyun reservoir (RW), sand-filtered water from Beijing drinking water treatment plant (FW), and secondary effluent from Qinghe wastewater treatment plant (WWTP), whose major quality parameters are summarized in Table S1.

2.3. Analysis

IPM was detected with an Agilent 1200 Series HPLC system equipped with an Atlantis C18 column (4.6 × 250 mm, 5.0 μm) at

UV wavelengths of 242 nm. The mobile phase was a mixture of methanol/water (85/15, v/v) at a flow rate of 1.0 mL min^{-1}. The injection volume was 50 μL, and the column temperature was maintained at 25 °C. The limit of quantitation of IPM by HPLC was determined to be 8.0 μg L^{-1}. IF was analyzed after samples being extracted with methyl *tert*-butyl ether using a gas chromatograph (7890, Agilent, CA, USA) equipped with an HP 5 capillary column (30 m × 0.25 mm, 0.25 μm, J&W, USA) and an electronic capture detector based on the modified USEPA method 551.1 (USEPA Method 551.1, 1995). I-HAAs were analyzed by liquid/liquid extraction with methyl-*tert*-butyl-ether (MtBE), derivatization with acidified methanol, and quantification by GC/ECD with the same capillary column based on the modified USEPA method 552.2 (USEPA Method 552.2, 1995). Iodate (IO_3^-) was quantified by an ion chromatograph (Dionex-ICS 2000) equipped with an Ionpac AS19 column (250 mm × 4.0 mm, 5.0 μm).

The high molecular weight transformation products (HMWTPs) of IPM by Fe(VI) oxidation were enriched by solid phase extraction (SPE) with an Oasis HLB cartridge (6 mL, 500 mg, Waters, Milford, MA, USA) at first. Detailed information on the SPE of samples is provided in Text S1. Then the extracts were identified by ultra-performance liquid chromatography-tandem quadrupole time-of-flight mass spectrometry (UPLC-QTOF-MS/MS, AcQuity LC, Xevo G2 QTOF MS, Waters, USA) coupled with an Eclipse Plus C18 column (2.1 × 150 mm, 3.5 μm, Agilent). The mobile phase consisted of 0.1% formic acid in water (A) and methanol (B) at a total flow rate of 0.3 mL min^{-1}. The gradient elution program (time in min, % mobile phase B) was set as follows: (0, 10), (15, 90), and (20, 10). Both the electrospray ionization$^+$ (ESI^+) and ESI^- modes were performed and compared at first for the products analysis. Because of the limited product detected under ESI^- mode, the MS system was operated at ESI^+ mode, cone voltage 30 V, capillary voltage 3 kV, desolvation temperature 280 °C, source temperature 100 °C, desolvation gas 500 L h^{-1}, and MS/MS collision energy 15–35 eV. The m/z range was from 100 to 800 and the scan time was 0.1 s. The molecular formula of a byproduct was determined by comparing the detected mass at a low collision voltage with the calculated mass according to the database of Masslynx 4.0 software. The chemical structures of some byproducts were also confirmed by their fragment spectra at a high collision voltage using the mass-fragment function in the software.

2.4. Computational details

In this work, the ground-state geometries and electronic structures of IPM were optimized by means of the hybrid density functional theory (DFT) method, using periodic boundary conditions, at the B3LYP level of theory with the 6-311++G (d,p) set performed on Gaussian 09 program package (Frisch et al., 2009). The optimization was repeated in solvent (water) described by the integral equation formalism polarizable continuum model (Cances et al., 1997). For the molecules which have more than one possible conformation, the conformation with the lowest electronic energy was singled out and adopted in the ensuing calculations. Frequency calculations were computed on these geometries at the same level to verify that they are real minimums on the potential energy surface without any imaginary frequency. The three-dimensional diagrams of optimized structure, the highest occupied molecular orbital (HOMO), (lowest unoccupied molecular orbital (LUMO), and the electrostatic potential were constructed with Gaussview.

3. Results and discussion

3.1. Oxidation kinetics of IPM by Fe(VI)

Generally, the oxidation kinetics of Fe(VI) are highly pH-dependent. Four protonation species for Fe(VI) exist in water (Eqs. (1)–(3)), which contribute to the reactivity variations in Fe(VI). For example, the redox potentials of monoprotonated Fe(VI) vary significantly (with +2.20 and + 0.72 V in acidic and alkaline circumstances, respectively) (Noorhasan et al., 2010; Yang et al., 2012; Kim et al., 2015). Thus, under lower pHs, Fe(VI) usually has higher redox potentials (Ramseier et al., 2011; Lee et al., 2014).

$$H_3FeO_4^+ \rightarrow H_2FeO_4 + H^+ \quad pK_1 = 1.5 \tag{1}$$

$$H_2FeO_4 \rightarrow HFeO_4^- + H^+ \quad pK_2 = 3.5 \tag{2}$$

$$HFeO_4^- \rightarrow FeO_4^{2-} + H^+ \quad pK_3 = 7.2 \tag{3}$$

The degradation kinetics of IPM by Fe(VI) were firstly investigated at pH 6.0–10.0. The evolution of normalized IPM concentration by Fe(VI) at pH 7.0 was shown in Fig. S1. The reaction of Fe(VI) with IPM under pseudo first-order conditions was tested and monitored. Plots of observed pseudo first-order rate constants (k_{obs}) showed linear relationships with concentrations of IPM in both acidic and alkaline circumstances ($R^2 \geq 0.99$). The degradation rate of IPM by Fe(VI) oxidation exhibited an obvious pH dependence, which can be attributed to the species-specific reactivity between Fe(VI) and IPM. The reactions between the two IPM species and four Fe(VI) species (eight in total) are further summarized with Eq. (4). Accordingly, k_{app} is given by Eq. (5).

$$\begin{aligned} d[IPM]_{tot}/dt &= k_{app}[Fe(VI)]_{tot}[IPM]_{tot} \\ &= \sum_{\substack{i=1,2,3,4 \\ j=1,2}} k_{ij}\alpha_i\beta_j[Fe(VI)]_{tot}[IPM]_{tot} \end{aligned} \tag{4}$$

$$k_{app} = \sum_{\substack{i=1,2,3,4 \\ j=1,2}} k_{ij}\alpha_i\beta_j \tag{5}$$

where k_{app} is the apparent second-order rate constant for the reaction of IPM with Fe(VI); $[Fe(VI)]_{tot} = [H_3FeO_4^+] + [H_2FeO_4] + [HFeO_4^-] + [FeO_4^{2-}]$, $[IPM]_{tot} = [IPM] + [IPM^-]$; α_i and β_j are the molar fraction of Fe(VI) and IPM; i and j are each of the four Fe(VI) species and two IPM species, respectively; and k_{ij} is the species-specific second-order rate constant for the reaction between the Fe(VI) species i with the IPM species j.

The kinetic model (Eq. (4)) could be further simplified based on the following facts: (1) the reaction related to FeO_4^{2-} could be neglected because of a much lower reactivity of FeO_4^{2-} than those of $HFeO_4^-$ and H_2FeO_4 (Dong et al., 2017b); and (2) only IPM^- ($pK_{IPM} = 4.5$), $HFeO_4^-$ and FeO_4^{2-} species were considered which dominated the IPM and Fe(VI) species at pH 6.0–10.0. Therefore, the reaction of IPM with Fe(VI) occurred predominantly between the anionic species of IPM and $HFeO_4^-$. As shown in Fig. 1, the modeled $k_{app,Fe(VI)\text{-}IPM}$ could match the measured $k_{app,Fe(VI)\text{-}IPM}$ value well. The obtained $k_{app,Fe(VI)\text{-}IPM}$ ranged from 0.7 M^{-1} s^{-1} to 74.6 M^{-1} s^{-1} at pH 6.0–10.0, which were highly dependent on pH. The $k_{app,Fe(VI)\text{-}IPM}$ at pH 7.0 was determined to be 55.8 M^{-1} s^{-1}. Meanwhile, the $k_{app,Fe(VI)\text{-}IPM}$ decreased significantly with increasing pH, which could be explained well by species-specific reactions between Fe(VI) species and IPM. The species-specific $k_{app,HFeO4^-\text{-}IPM}$ of the reaction of $HFeO_4^-$ with IPM^- was

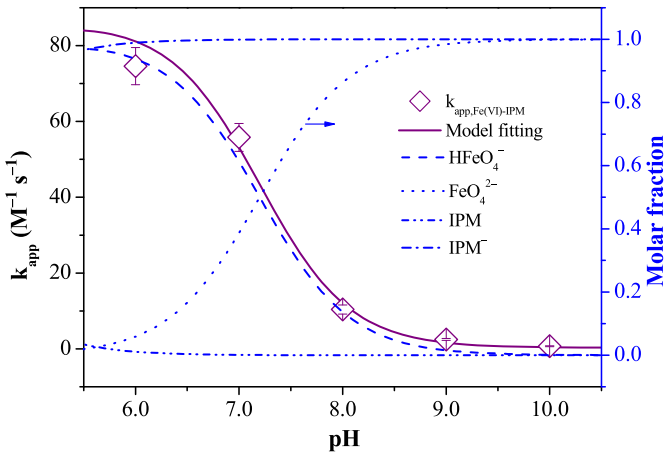

Fig. 1. Model fitting of the second-order reaction rate constant of IPM with Fe(VI) as a function of solution pH. Experimental conditions: $[Fe(VI)]_o$ = 0.1–0.5 mM, $[IPM]_o$ = 10 μM, reaction time = 30 min, pH 6.0–10.0, 25 °C. Error bars represent the 95% confidence interval. IPM: iopamidol.

determined to be 86.5 M^{-1} s^{-1}, respectively via least-squares nonlinear regressions ($R^2 > 0.99$), significantly higher than that of the reaction with FeO_4^{2-} and IPM^- (0.19 M^{-1} s^{-1}). The contribution of main species to the overall reaction rate at pH 6.0–10.0 could be modeled with these species-specific k_{app} values. The contribution of $HFeO_4^-$ overweighed H_2FeO_4 and FeO_4^{2-} during the oxidation of IPM by Fe(VI) at pH 6.0–10.0. Ning and Graham (2008) reported the k_{app} range for IPM with hydroxyl radical were in the range of 1.0×10^9–3.0×10^9 M^{-1} s^{-1}. Chlorination of IPM followed a second order reaction, with a k_{app} value up to 0.87 M^{-1} s^{-1} (±0.021 M^{-1} s^{-1}) at pH 8.5 (Wendel et al., 2014). Overall, the k_{app} values for IPM with Fe(VI) were obviously lower than hydroxyl radical, while comparable to mild hypochlorite.

3.2. Formation of I-DBPs during the oxidation of IPM by Fe(VI)

I-DBP formation during the oxidation of IPM by Fe(VI) was investigated as a function of time. Fig. 2 shows the evolution of I-DBPs during the oxidation of IPM by Fe(VI). As Fe(VI), IPM and NOM did not include chlorine (Cl) and bromine (Br) elements, Cl- or Br-containing I-DBPs would not form in this study and the observed I-DBPs species were IF, IAA and TIAA. After 1 h, all the IF, IAA and TIAA formations were detected. During the whole time course, the formation of IF was always far higher than those of IAA and TIAA. After 72 h, the average IF formation reached 64.29 ± 7.04 μg L^{-1}, whereas the IAA and TIAA formation concentrations were only 1.70 ± 0.36 μg L^{-1} and 9.59 ± 0.90 μg L^{-1}, respectively. Meanwhile, IF, IAA and TIAA exhibited different formation rates during the 72 h time course. The IF and TIAA concentrations increased with increasing time, whereas the IAA concentration reached their maximum values after 12 h (i.e., 2.10 ± 0.15 μg L^{-1}). Then a decreasing trends of IAA concentration was observed. This decrease of IAA concentration during chloramination as a function of time was also observed by Liu et al. (2017), probably due to its transformation into TIAA in the presence of excess IPM. Overall, the different IF, IAA and TIAA concentrations formed during the oxidation of IPM by Fe(VI) could be attributed to their relative stabilities and formation pathways (Chu et al., 2009).

Fig. 3 shows the formation of IF, IAA and TIAA as a function of IPM dose after 72 h. It was found that the formation of I-DBPs was increased with increasing levels of IPM (10–50 μM). For example, the formation of IF increased from 3.47 ± 0.56 μg L^{-1} to 64.29 ± 7.04 μg L^{-1} with the initial IPM concentration increased from 10 to 50 μM. However, when the initial IPM concentration reached 100 μM, the formation of I-DBPs decreased slightly. Liu et al. (2017) observed a similar trend that the formation of I-DBPs during chloramination exhibited a decreasing trend when the initial I^- concentration reached higher than 200 μM. Like I^-, excess IPM also could compete for Fe(VI) for the formation of free iodine. Therefore, the molar ratio of IPM to Fe(VI) is critical for the free iodine formation and transformation into I-DBPs during oxidation.

As mentioned, the chemical reactivity of H_2FeO_4, $HFeO_4^-$, and FeO_4^{2-} reduced in order. With pHs increase from 6.0 to 10.0, the constitution of Fe(VI) species changed from H_2FeO_4 to $HFeO_4^-$ and FeO_4^{2-}, which influenced not only the degradation kinetics of IPM, but also the formation of I-DBPs. The formation of I-DBPs during the oxidation of IPM by Fe(VI) was further investigated at pH 6.0–10.0 (Fig. 4). It was found that the formation of I-DBPs during the oxidation of IPM was affected significantly by solution pH. The highest formation of I-DBPs was observed at pH 9.0. With the increase of pH from 6.0 to 9.0, the summed formation amounts of I-DBPs increased from 5.42 ± 0.95 μg L^{-1} to 75.59 ± 8.23 μg L^{-1}. The formation of I-DBPs decreased slightly when pH increased from 9.0

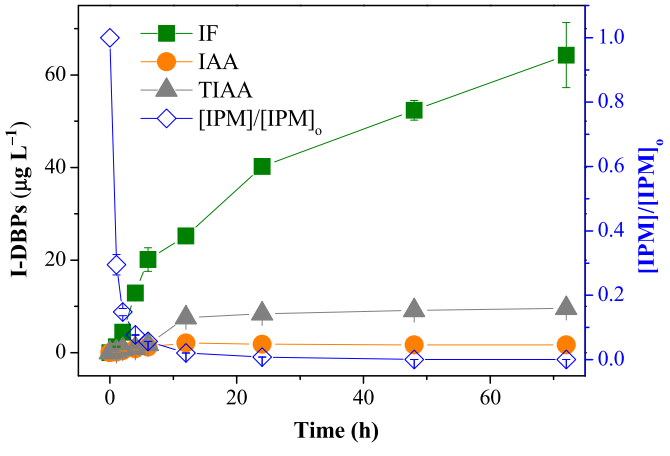

Fig. 2. Evolution of I-DBPs and normalized IPM concentration as a function of reaction time during oxidation of IPM by Fe(VI). Experimental conditions: $[Fe(VI)]_o$ = 0.5 mM, $[NOM]_o$ = 0.5 mgC L^{-1}, $[IPM]_o$ = 50 μM, pH 9.0, 25 °C. Error bars represent the 95% confidence interval.

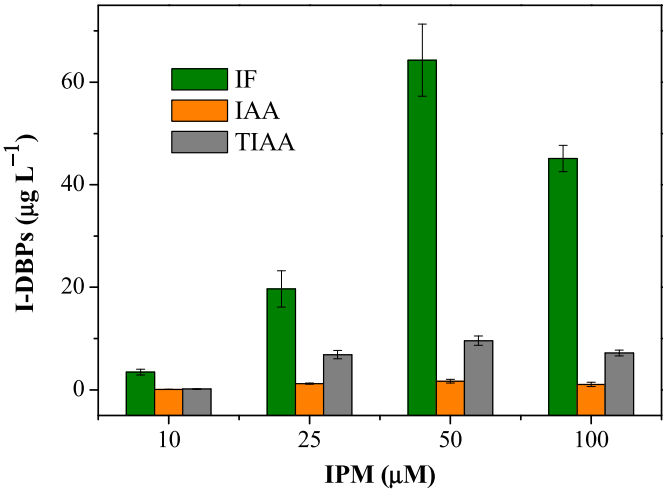

Fig. 3. Effect of initial IPM concentration on I-DBP formation during oxidation of IPM by Fe(VI). Experimental conditions: $[Fe(VI)]_o$ = 0.5 mM, $[NOM]_o$ = 0.5 mgC L^{-1}, reaction time = 72 h, pH 9.0, 25 °C. Error bars represent the 95% confidence interval.

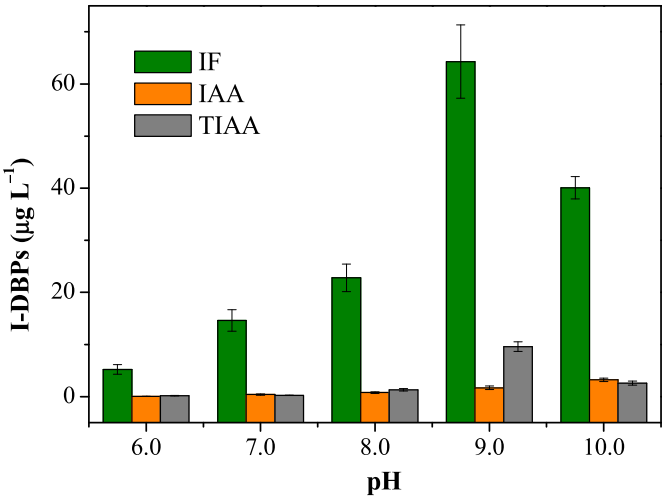

Fig. 4. Effect of pH on I-DBP formation during oxidation of IPM by Fe(VI). Experimental conditions: $[Fe(VI)]_o$ = 0.5 mM, $[NOM]_o$ = 0.5 mgC L^{-1}, $[IPM]_o$ = 50 μM, reaction time = 72 h, 25 °C. Error bars represent the 95% confidence interval.

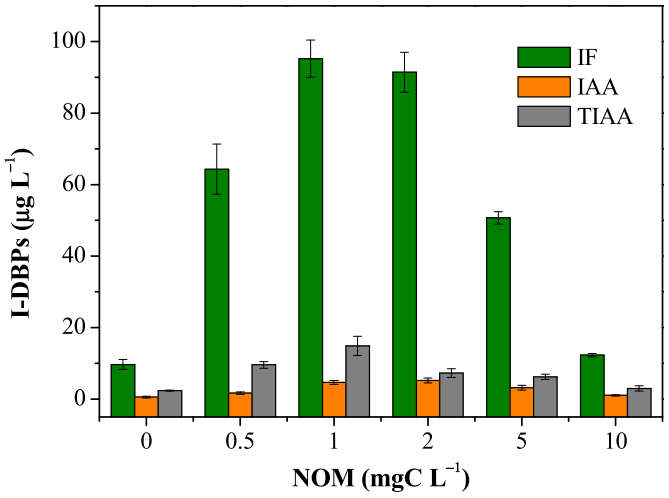

Fig. 5. Effect of initial NOM concentration on I-DBP formation during oxidation of IPM by Fe(VI). Experimental conditions: $[Fe(VI)]_o$ = 0.5 mM, $[IPM]_o$ = 50 μM, reaction time = 72 h, pH 9.0, 25 °C. Error bars represent the 95% confidence interval.

to 10.0. The pH-dependent formation trend of I-DBPs may be attributed to pH-dependent reactivity of Fe(VI). Kralchevska et al. (2016) reported the second-order rate constants between Fe(VI) and I^- ($k_{app,Fe(VI)\text{-}I^-}$) decreased from 3.9 × 10^4 M^{-1} s^{-1} at pH 5.0–12 M^{-1} s^{-1} at pH 10.3. Zhang et al. (2016) also found that Fe(VI) could oxidized I^- into IO_3^- under acidic and neutral circumstances. With the increase of pH from 6.0 to 10.0, the IO_3^- formation amounts during the oxidation of IPM by Fe(VI) decreased significantly from 1215 ± 29.6 μg L^{-1} to 127 ± 8.7 μg L^{-1} (Fig. S2). Thus, the I^- from the deiodination of IPM by Fe(VI) was oxidized partly into IO_3^- under acidic and neutral circumstances, which subsequently limited the formation of I-DBPs. As shown in Fig. S2, the dominant fate of iodine after the oxidation by Fe(VI) was total organic iodine in the TBPs of IPM. Previous study showed similar results with transformation molar ratio of IPM to I-DBPs around 2% (Duirk et al., 2011).

The formation of I-DBPs during the oxidation of IPM by Fe(VI) was hypothesized: (1) released I^- is oxidized to HOI by Fe(VI); (2) the formed HOI reacts with NOM moieties via electrophilic substitution to form iodinated products or oxidizes NOM moieties via electron transfer (Criquet et al., 2015). To evaluate the role of NOM on the formation of I-DBPs, the effect of NOM concentration (0–10 mgC L^{-1}) was studied in Fig. 5. During the oxidation of IPM by Fe(VI), I-DBPs was formed even in the absence of NOM. It was speculated that the TBPs of IPM may become carbon precursors of I-DBPs. However, the formation amount of I-DBPs in absence of NOM is obviously lower than those in the presence of NOM (0.5–5 mgC L^{-1}). When 1.0 mgC L^{-1} was added to the oxidation system, the IF, IAA and TIAA formation after 72 h increased from 9.7 ± 1.4 μg L^{-1}, 0.6 ± 0.1 μg L^{-1} and 2.4 ± 0.1 μg L^{-1} to 95.2 ± 5.2 μg L^{-1}, 4.70 ± 0.6 μg L^{-1} and 14.9 ± 2.7 μg L^{-1}, respectively. When the NOM concentration exceeded 1.0 mgC L^{-1}, the formation of I-DBPs exhibited a decreasing trend. The chemical structure of NOM and its DBPs formation potential after Fe(VI) oxidation could be changed (Gan et al., 2015). Although NOM acted as the main precursor for the I-DBPs during the oxidation of IPM by Fe(VI), excess NOM may compete with IPM for Fe(VI), which subsequently reduces the formation of free iodine and I-DBPs.

3.3. Transformation pathways of IPM by Fe(VI) oxidation

UPLC-QTOF-MS/MS analysis was adopted to investigate the HMWTPs of IPM by Fe(VI). As shown in Fig. S3 and Table S2, ten HMWTPs (i.e., IPM705, IPM661, IPM651, IPM631, IPM609, IPM579, IPM535, IPM483, IPM453, IPM409) were identified after the oxidation of IPM by Fe(VI). On the basis of these identified HMWTPs, tentative pathways for the reactions of IPM with Fe(VI) were proposed. Overall, the transformation of IPM by Fe(VI) oxidation was tentatively ascribed to three pathways (Fig. 6): (1) deiodination; (2) amide hydrolysis; and (3) oxidation of amine (Hu et al., 2017). Deiodination from IPM is the prerequisite for the formation of I-DBPs during the oxidation of IPM. Jeong et al. (2010) observed the deiodination reaction during the degradation of ICMs by advanced oxidation processes. It also has been reported that an iodo-group had a higher potential to leave than a chloro-group (Woo et al., 2002). In this study, the identification of IPM651, IPM535, IPM483 and IPM409 verified that the deiodination reaction took place during the oxidation of IPM by Fe(VI), which facilitated the formation of free iodine and I-DBPs. Hu et al. (2017) reported the amide hydrolysis of IPM side chain during peroxymonosulfate oxidation. In this study, amide hydrolysis and subsequent amine oxidation of IPM side chain also occurred, yielding IPM705, IPM631, IPM661 and IPM409.

In a previous study, Wendel et al. (2014) identified 19 HMWTPs after the chlorination of IPM. They further isolated and identified five HMWTPs and compared their cytotoxicity and genotoxicity using mammalian cells with I-DBPs. It was further found that, four of the five HMWTPs exhibited low levels of cytotoxicity, whereas not one of the HMWTPs was genotoxic (Wendel et al., 2016), indicating that these 10 HMWTPs identified in this study were not the forcing agents that induced cytotoxicity and genotoxicity. The formation of small-molecular-weight I-DBPs (i.e., IF, IAA and TIAA) during the oxidation of IPM by Fe(VI) are speculated to be responsible for the toxicity change, which needs to be given sufficient attention.

3.4. Formation of I-DBPs during the oxidation of ICMs by Fe(VI)

The effect of Fe(VI) oxidation on the formation of I-DBPs was further evaluated for three different ICMs including iohexol, diatrizoate, and iopromide. Similar to IPM, iohexol, diatrizoate, and iopromide formed IF, IAA and TIAA during the Fe(VI) oxidation in the presence of 0.5 mgC L^{-1}. But, unlike IPM, which produced significant levels of I-DBPs up to 75.6 μg L^{-1}, iohexol, diatrizoate and

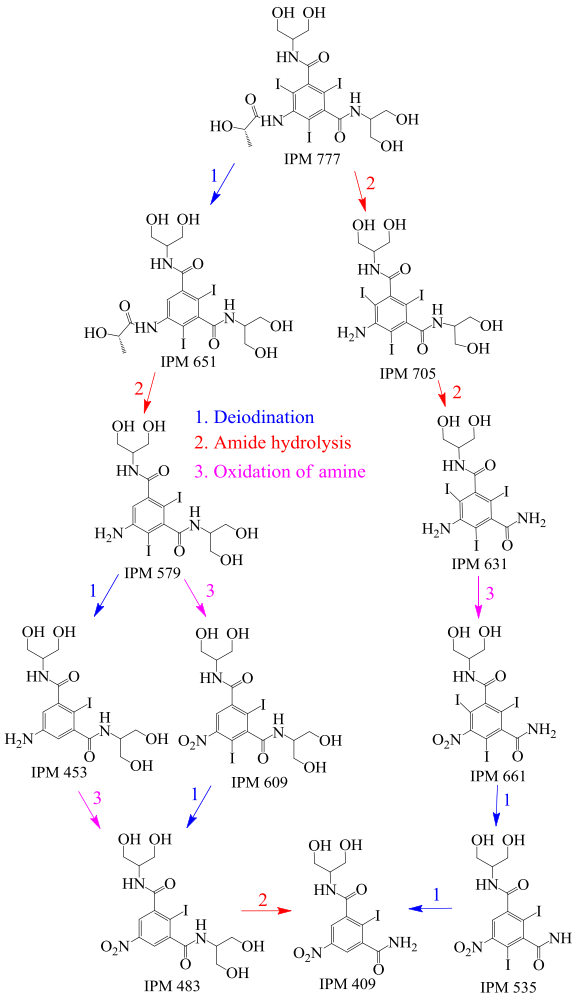

Fig. 6. Degradation pathways of IPM by Fe(VI) oxidation.

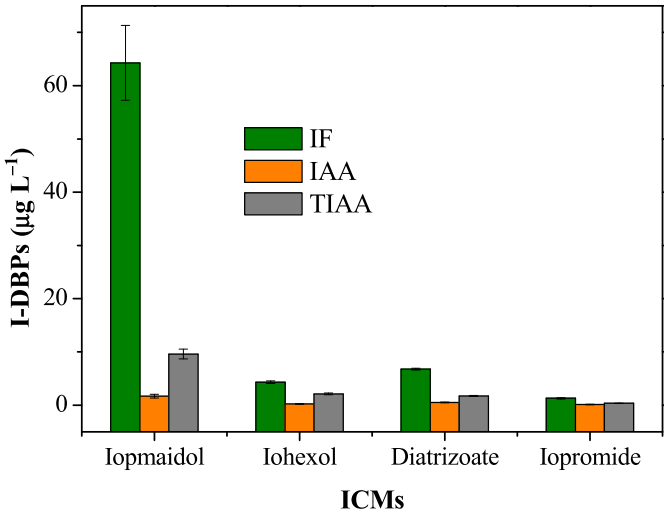

Fig. 7. Formation of I-DBPs during oxidation of different ICMs by Fe(VI). Experimental conditions: $[Fe(VI)]_o$ = 0.5 mM, $[IPM]_o$ = 50 μM, $[NOM]_o$ = 0.5 mg L^{-1}, reaction time = 72 h, pH 9.0, 25 °C. Error bars represent the 95% confidence interval.

iopromide did not form appreciable levels (<10.0 μg L^{-1}). Duirk et al. (2011) observed similar results that the formation amounts of I-DBPs from iohexol and iopromide were rather limited when treated with chlorine or monochloramine. Thus, it seems that IPM has the highest chemical reactivity for Fe(VI) oxidation among the four ICMs.

Frontier orbital theory analysis, which was considered as a reliable tool for the analysis of chemical reactivity, was adopted to reveal the of I-DBP formation difference from the four ICMs (Aihara, 1999). In frontier orbital theory, HOMO and LUMO determine the way a molecule interacts with other species. HOMO–LUMO energy gap is widely adopted in molecule reactivity analysis (Kumar et al., 2015). As shown in Fig. 8, it was found that the HOMO of IPM was contracted and shifted mainly towards the heterocyclic ring which primarily acts as an electron donor, whereas the LUMO of IPM was distributed almost uniformly, which acts as an electron acceptor. The HOMO–LUMO energy gap of IPM was 3.94 eV, while those of iohexol, diatrizoate and iopromide were 4.43, 4.23 and 4.69 eV, respectively (Figs. S4–6). The HOMO-LUMO energy gap results were consistent with the highest formation potential of I-DBPs during the ICMs oxidation by Fe(VI) in Fig. 7.

3.5. Formation of I-DBPs in real water samples

To evaluate the effect of water matrix on the I-DBP formation during the oxidation of IPM by Fe(VI), three real samples from a wastewater treatment plant (WWTP) effluent, river water (RW) and filtered water from a drinking water treatment plant (DW) spiked with 500 μg L^{-1} IPM were tested at pH 8.5. Due to their different DOC contents, the concentrations of I-DBPs were normalized by the DOC concentration. As shown in Fig. 9, IF, IAA and TIAA were all observed after 72 h. For all the three tested water samples, the formation amounts of IF were always higher than those of IAA and TIAA. For example, all the normalized IF formation amounts were >1.0 μg mgC^{-1}, while those of IAA and TIAA were <1.0 μg mgC^{-1}. Overall, the DOC-normalized total yield of I-DBPs in

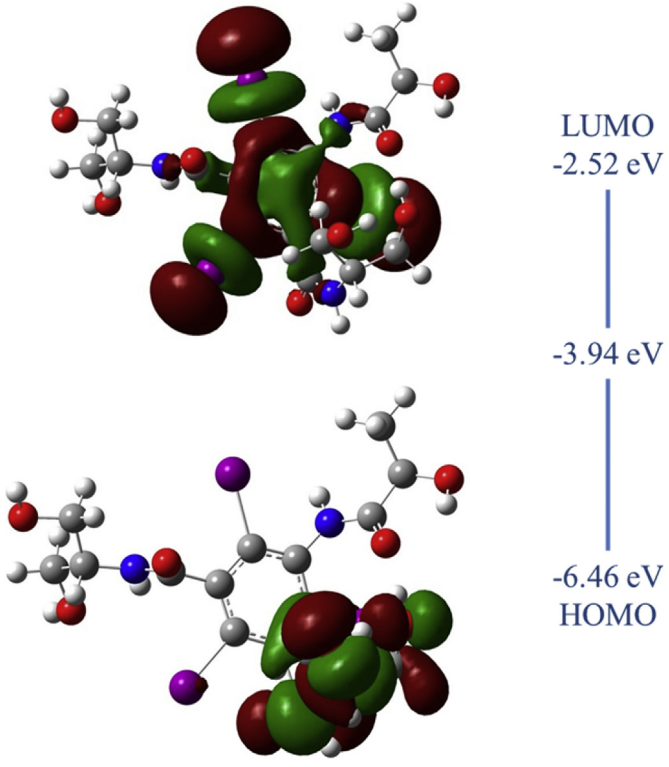

Fig. 8. HOMO–LUMO plot of IPM molecular obtained by B3LYP/6-311++G (d,p) level.

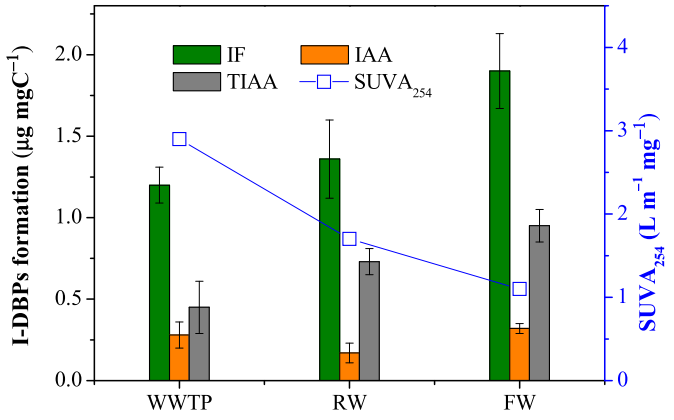

Fig. 9. Formation of I-DBPs during oxidation of IPM by Fe(VI) in real water samples. Experimental conditions: $[Fe(VI)]_o$ = 5.0 mg L^{-1}, $[IPM]_o$ = 500 μg L^{-1}, reaction time = 72 h, pH 8.0, 25 °C. Error bars represent the 95% confidence interval. WWTP: wastewater treatment plant effluent; RW: river water; FW: filtered water in a drinking water treatment plant.

the three real waters followed the descending order of FW > RW > WWTP, which may be attributable to their different DOC contents. The specific ultraviolet absorbance at 254 nm ($SUVA_{254}$) is widely adopted as an indicator of aromatic content and DBP formation potential of organic matter. From the limited dataset in this study, it appears that low-$SUVA_{254}$ NOM was more reactive in the I-DBP formation during the oxidation of IPM by Fe(VI) than high-$SUVA_{254}$ NOM. High-$SUVA_{254}$ NOM may compete with IPM for Fe(VI), which limits the oxidation process of IPM and subsequent I-DBP formation.

As IPM widely exists in the wastewater, surface water and even drinking water, the kinetic parameters in this study are useful for the selection and optimization of advanced process to eliminate IPM concentration. Moreover, the formation of I-DBPs during the oxidation of IPM by Fe(VI) was of great interest because Fe(VI) is usually considered as one of the few oxidants that seldom forms halogenated hazardous byproducts. The formation of I-DBPs in this study could provide insights to evaluate I-DBP formation mechanism and pathway during the oxidation of inorganic and organic iodine in future.

4. Conclusions

Based on the experimental results, the following conclusions can be drawn:

- The obtained k_{app} for the oxidation of IPM with Fe(VI) ranged from 0.7 M^{-1} s^{-1} to 74.6 M^{-1} s^{-1} at pH 6.0–10.0 and $HFeO_4^-$ and the IPM^- species control the overall reaction.
- The oxidation of IPM by Fe(VI) led to the formation of toxic IF, IAA and TIAA and maximum formation of I-DBPs occurred at pH 9.0.
- Deiodination reaction during the oxidation of IPM by Fe(VI) contributed to the formation of I-DBPs.
- Because of its lowest HOMO–LUMO energy gap among the four investigated ICMs, IPM exhibited the highest formation of I-DBPs during Fe(VI) oxidation.

Acknowledgment

This work was financially supported by the National Natural Science Foundation of China (51408590, 51290281, 51525806), Chinese Academy of Sciences (QYZDY-SSW-DQC004), Ministry of Housing and Urban-Rural Development of China (2017ZX07207-004) and CAS/SAFEA International Partnership Program for Creative Research Teams of China.

Appendix A. Supplementary data

Supplementary data related to this article can be found at https://doi.org/10.1016/j.watres.2017.12.003.

References

Aihara, J., 1999. Reduced HOMO-LUMO gap as an index of kinetic stability for polycyclic aromatic hydrocarbons. J. Phys. Chem. A 103, 7487–7495.
Anquandah, G.A.K., Sharma, V.K., Knight, D.A., Batchu, S.R., Gardinali, P.R., 2011. Oxidation of trimethoprim by ferrate(VI): kinetics, products, and antibacterial activity. Environ. Sci. Technol. 45, 10575–10581.
Cances, E., Mennucci, B., Tomasi, J., 1997. A new integral equation formalism for the polarizable continuum model: theoretical background and applications toisotropic and anisotropic dielectrics. J. Chem. Phys. 107, 3032–3041.
Christiansen, C., 2005. X-ray contrast media-an overview. Toxicology 209, 185–187.
Chu, W.H., Gao, N.Y., Deng, Y., 2009. Stability of newfound nitrogenous disinfection by-products haloacetamides in drinking water. Chin. J. Org. Chem. 29, 1569–1574.
Criquet, J., Rodriguez, E.M., Allard, S., Wellauer, S., Salhi, E., Joll, C.A., von Gunten, U., 2015. Reaction of bromine and chlorine with phenolic compounds and natural organic matter extracts-Electrophilic aromatic substitution and oxidation. Water Res. 85, 476–486.
Dong, H.Y., Qiang, Z.M., Hu, J., Sans, C., 2017a. Accelerated degradation of iopamidol in iron activated persulfate systems: roles of complexing agents. Chem. Eng. J. 316, 288–295.
Dong, H.Y., Qiang, Z.M., Lian, J.F., Qu, J.H., 2017b. Promoted oxidation of diclofenac with ferrate (Fe(VI)): role of ABTS as the electron shuttle. J. Hazard. Mater. 336, 65–70.
Duirk, S.E., Lindell, C., Cornelison, C.C., Kormos, J., Ternes, T.A., Attene-Ramos, M., Osiol, J., Wagner, E.D., Plewa, M.J., Richardson, S.D., 2011. Formation of toxic iodinated disinfection by-products from compounds used in medical imaging. Environ. Sci. Technol. 45, 6845–6854.
Eversloh, C.L., Henning, N., Schulz, M., Ternes, T.A., 2014. Electrochemical treatment of iopromide under conditions of reverse osmosis concentrates-Elucidation of the degradation pathway. Water Res. 48, 237–246.
Frisch, M.J., Trucks, G.W., Schlegel, H.B., Scuseria, G.E., Robb, M.A., Cheeseman, J.R., Scalmani, G., Barone, V., Mennucci, B., 2009. Gaussian 09, Revision D.01. Gaussian, Inc, Wallingford, CT.
Gan, W.H., Sharrna, V.K., Zhang, X., Yang, Y., Yang, X., 2015. Investigation of disinfection byproducts formation in ferrate(VI) pre-oxidation of NOM and its model compounds followed by chlorination. J. Hazard. Mater. 292, 197–204.
Hu, J., Dong, H.Y., Qu, J.H., Qiang, Z.M., 2017. Enhanced Degradation of Iopamidol by Peroxymonosulfate Catalyzed by Two Pipe Corrosion Products (CuO and δ-MnO_2), vol. 112, pp. 1–8.
Jeong, J., Jung, J., Cooper, W.J., Song, W.H., 2010. Degradation mechanisms and kinetic studies for the treatment of X-ray contrast media compounds by advanced oxidation/reduction processes. Water Res. 44, 4391–4398.
Jiang, J.Q., Wang, S., 2003. Enhanced coagulation with potassium ferrate(VI) for removing humic substances. Environ. Eng. Sci. 20, 627–633.
Kim, C., Panditi, V.R., Gardinali, P.R., Varma, R.S., Kim, H., Sharma, V.K., 2015. Ferrate promoted oxidative cleavage of sulfonamides: kinetics and product formation under acidic conditions. Chem. Eng. J. 279, 307–316.
Kralchevska, R.P., Sharma, V.K., Machala, L., Zboril, R., 2016. Ferrates (Fe-VI, Fe-V, and Fe-IV) oxidation of iodide: formation of triiodide. Chemosphere 144, 1156–1161.
Kormos, J.L., Schulz, M., Wagner, M., Ternes, T.A., 2009. Multistep approach for the structural identification of biotransformation products of iodinated X-ray contrast media by liquid chromatography/hybrid triple quadrupole linear ion trap mass spectrometry and ^{1}H and ^{13}C nuclear magnetic resonance. Anal. Chem. 81, 9216–9224.
Kormos, J.L., Schulz, M., Kohler, H.P.E., Ternes, T.A., 2010. Biotransformation of selected iodinated X-ray contrast media and characterization of microbial transformation pathways. Environ. Sci. Technol. 44, 4998–5007.
Kumar, A., Srivastava, A.K., Gangwar, S., Misra, N., Mondal, A., Brahmachari, G., 2015. Combined experimental (FT-IR, UV–visible spectra, NMR) and theoretical studies on the molecular structure, vibrational spectra, HOMO, LUMO, MESP surfaces, reactivity descriptor and molecular docking of Phomarin. J. Mol. Struct. 1096, 94–101.
Lee, Y., Kissner, R., von Gunten, U., 2014. Reaction of ferrate(VI) with ABTS and self-decay of ferrate(VI): kinetics and mechanisms. Environ. Sci. Technol. 48, 5154–5162.
Liu, S.G., Li, Z.L., Dong, H.Y., Goodman, B.A., Qiang, Z.M., 2017. Formation of iodotrihalomethanes, iodo-acetic acids, and iodo-acetamides during chloramination of iodide-containing waters: factors influencing formation and reaction pathways. J. Hazard. Mater. 321, 28–36.
Matsushita, T., Kobayashi, N., Hashizuka, M., Sakuma, H., Kondo, T., Matsui, Y.,

Shirasaki, N., 2015. Changes in mutagenicity and acute toxicity of solutions of iodinated X-ray contrast media during chlorination. Chemosphere 135, 101–107.
Ning, B., Graham, N.J.D., 2008. Ozone degradation of iodinated pharmaceutical compounds. J. Environ. Eng. 134, 944–953.
Noorhasan, N., Patel, B., Sharma, V.K., 2010. Ferrate(VI) oxidation of glycine and glycylglycine: kinetics and products. Water Res. 44, 927–935.
Perez, S., Barcelo, D., 2007. Fate and occurrence of X-ray contrast media in the environment. Anal. Bioanal. Chem. 387, 1235–1246.
Ramseier, M.K., Peter, A., Traber, J., von Gunten, U., 2011. Formation of assimilable organic carbon during oxidation of natural waters with ozone, chlorine dioxide, chlorine, permanganate, and ferrate. Water Res. 45, 2002–2010.
Richardson, S.D., Fasano, F., Ellington, J.J., Crumley, F.G., Buettner, K.M., Evans, J.J., Blount, B.C., Silva, L.K., Waite, T.J., Luther, G.W., 2008. Occurrence and mammalian cell toxicity of iodinated disinfection byproducts in drinking water. Environ. Sci. Technol. 42, 8330–8338.
Rush, J.D., Zhao, Z., Bielski, B.H.J., 1996. Reaction of ferrate(VI)/ferrate(V) with hydrogen peroxide and superoxide anion-a stopped-flow and premix pulse radiolysis study. Free Radic. Res. 24, 187–198.
Schulz, M., Loffler, D., Wagner, M., Ternes, T.A., 2008. Transformation of the X-ray contrast medium iopromide in soil and biological wastewater treatment. Environ. Sci. Technol. 42, 7207–7217.
Seitz, W., Jiang, J.Q., Weber, W.H., Lloyd, B.J., Maier, M., Maier, D., 2006. Removal of iodinated X-ray contrast media during drinking water treatment. Environ. Chem. 3, 35–39.
Seitz, W., Jiang, J.Q., Schulz, W., Weber, W.H., Maier, D., Maier, M., 2008. Formation of oxidation by-products of the iodinated X-ray contrast medium iomeprol during ozonation. Chemosphere 70, 1238–1246.
Sharma, V.K., O'Connor, D.B., Cabelli, D.E., 2001. Sequential one-electron reduction of Fe(V) to Fe(III) by cyanide in alkaline medium. J. Phys. Chem. B 105, 11529–11532.
Sharma, V.K., 2007. Disinfection performance of Fe(VI) in water and wastewater: a review. Water Sci. Technol. 55, 225–232.
Simazaki, D., Kubota, R., Suzuki, T., Akiba, M., Nishimura, T., Kunikane, S., 2015. Occurrence of selected pharmaceuticals at drinking water purification plants in Japan and implications for human health. Water Res. 76, 187–200.
USEPA Method 551.1, 1995. Determination of Chlorination Disinfection by products, Chlorinated Solvents, and Halogenated Pesticides/herbicides in Drinking Water by Liquid-liquid Extraction and Gas Chromatography with Electron-capture Detection. National Exposure Research Laboratory Office of Research and Development, Cincinnati, Ohio, USA.
USEPA Method 552.2, 1995. Determination of Haloacetic Acids and Dalapon in Drinking Water by Liquid-liquid Extraction, Derivatization and Gas Chromatography with Electron Capture Detection. National Exposure Research Laboratory Office of Research and Development, Cincinnati, Ohio, USA.
Wendel, F.M., Eversloh, C.L., Machek, E.J., Duirk, S.E., Plewa, M.J., Richardson, S.D., Ternes, T.A., 2014. Transformation of iopamidol during chlorination. Environ. Sci. Technol. 48, 12689–12697.
Wendel, F.M., Ternes, T.A., Richardson, S.D., Duirk, S.E., Pals, J.A., Wagner, E.D., Plewa, M.J., 2016. Comparative toxicity of high-molecular weight iopamidol disinfection byproducts. Environ. Sci. Tech. Let. 3, 81–84.
Woo, Y.T., Lai, D., McLain, J.L., Manibusan, M.K., Dellarco, V., 2002. Use of mechanism-based structure-activity relationships analysis in carcinogenic potential ranking for drinking water disinfection by-products. Environ. Health Perspect. 110, 75–87.
Yang, B., Ying, G.G., Zhao, J.L., Liu, S., Zhou, L.J., Chen, F., 2012. Removal of selected endocrine disrupting chemicals (EDCs) and pharmaceuticals and personal care products (PPCPs) during ferrate(VI) treatment of secondary wastewater effluents. Water Res. 46, 2194–2204.
Yang, M.T., Zhang, X.R., 2013. Comparative developmental toxicity of new aromatic halogenated DBPs in a chlorinated saline sewage effluent to the marine polychaete platynereis dumerilii. Environ. Sci. Technol. 47, 10868–10876.
Zhang, M.S., Xu, B., Wang, Z., Zhang, T.Y., Gao, N.Y., 2016. Formation of iodinated trihalomethanes after ferrate pre-oxidation during chlorination and chloramination of iodide-containing water. J. Taiwan Inst. Chem. E 60, 453–459.